Photocatalytic Hydrogen from Water Over Semiconductors

Siow Hwa Teo, Aminul Islam, and Yun Hin Taufiq-Yap

Abstract Water splitting to produce hydrogen (H_2) over a semiconductor photocatalyst using solar energy is a promising process for the large-scale production of clean chemical energy in the form of H_2, a clean and renewable energy carrier. Many efforts have been implemented to discover photocatalysts that workable under visible-light irradiation to efficiently utilize solar energy. Generally, a suitable cocatalyst to provide an active redox site, is a recognize manner to modify the water-splitting photocatalysts. Apart from that, the constructed two-step photoexcitation photocatalysts, mimicking the natural photosynthesis system, using two different semiconductor powder, have many merits, including amplified light harvesting, spatially separated reductive and oxidative active sites, and perfectly preserved powerful redox ability, which advantage the photocatalytic performance. Especially, a photocatalytic framework called Z-scheme, which is fundamentally comprises of a H_2-photocatalyst and an O_2-photocatalyst to perform water reduction and oxidation, individually. This chapter describe the fundamental development of water-splitting photocatalytic systems.

Keywords Semiconductor · Water-splitting photocatalyst · Cocatalyst · Z-scheme · H_2 evolution

S. H. Teo (✉) · Y. H. Taufiq-Yap (✉)
Faculty of Science and Natural Resources, Universiti Malaysia Sabah, Jalan UMS, 88400 Kota Kinabalu, Sabah, Malaysia
e-mail: tony@ums.edu.my

Y. H. Taufiq-Yap
e-mail: taufiqyap@ums.edu.my

A. Islam
Department of Petroleum and Mining Engineering, Jashore University of Science and Technology, Jashore 7408, Bangladesh

A. Gupta et al. (eds.), *Advances in Energy and Combustion*, Green Energy and Technology,
https://doi.org/10.1007/978-981-16-2648-7_8

Nomenclature

.

$A_{\text{Geometric}}$	Area of reactor
E_c	Conductive band minimum
E_F	Fermi level
$E\text{H}_2/\text{H}_2\text{O}$	Hydrogen evolution potential
$E\text{O}_2/\text{H}_2\text{O}$	Oxygen evolution potential
E_v	Valence band maximum
E_v	Planck's constant
I_{light}	Irradiance intensity at λ
I_{o}	Power density of incident light
j_{p}	Photocurrent density at the measured potential
J	Photocurrent density at 0 V at a certain wavelength
P_{sun}	Energy free of sunlight
v	Frequency
V	Voltage
v_{ac}	Vacuum level
$r\text{H}_2$	Hydrogen production rate
V	Bias potential
W	Work function
ΔG	Gibbs free energy
λ	Wavelength
λ	Wavelength

Abbreviations

Ag	Silver
Au	Gold
Br	Bromide
Br_2	Bromine
C	Carbon
CB	Conductive band
CH_4	Methane
CNTs	Carbon nanotubes
CO_2	Carbon dioxide
Cu	Copper
Cu_2O	Copper oxide
DMF	Dimethyl fluoride
EQN	Equation
g-C3N4	Graphitic carbon nitride

GO	Graphene oxide
HER	Hydrogen evolution reaction
HI	Hydrogen iodine
H_2	Hydrogen
H_2O	WaterWater
IPCE	Incident photon to current conversion efficiency
MoS_2	Molybdenum disulfide
NHE	Normal hydrogen electrode
Nd_2O_5	Neodymium oxide
NiO	Nickel oxide
NPs	Nanoparticles
OER	Oxygen evolution band
O_2	Oxygen
pH	Potential of hydrogen or power of hydrogen
PC	Photocatalyst
PCE	Photo conversion efficiency
Pt	Platinum
QE	Quantum efficiency
RuO_2	Ruthenium oxide
SHT	Solar to hydrogen
Si	Silicon
$SrTiO_3$	Strontium titanium oxide
THF	Tetrahydrofuran
TiO_2	Titanium oxide
UV	Ultraviolet
VB	Valence band
WO_3	Tungsten oxide
vs.	Versus
Zno	Zinc oxide
2D	Two dimensional

1 Introduction

Solar energy is considered as most promising candidate to substitute the fossil fuels. It also leads us to achieve clean, sustainable and environment friendly fuel and it is predicted that only 0.01% solar energy conversion can be enough to solve the world's energy crisis [1, 2]. The most abundant component across the universe, hydrogen (H_2) is burned to generated only water (H_2O) and hence it is reflected as a perspective clean energy source for the future once it can be made inexpensively and expeditiously [3, 4]. One of the best way to keep and manage the solar energy is photocatalysis which stores energy in the form of chemical fuel [5]. Therefore, solar H_2 production can attain directly from H_2O splitting process using solar energy as driving force to split

water molecules to H_2 and oxygen (O_2) on the surface of catalyst. Additionally, the method is also as source for O_2, carbon dioxide (CO_2) and methane (CH_4), which are the products for other fuel production routes [6].

In 1972, photocatalytic water splitting was emerged, which the first report is authorized by Fujishima and Honda [9] using a photoelectrochemical system. Through the report published in Nature, suggesting that the H_2O molecule is oxidized via photoinduced holes on TiO_2 surface with the assistant of small electrical voltage, until near recent twentieth century, it witnessed the nonstop progression of photocatalysis [2, 5, 8, 10] including photocatalytic water splitting on powder photocatalyst particles. An overall photocatalytic water splitting process (based on semiconductor) typically includes three essential steps [10], (1) absorption of light followed by electron–hole separation inside the semiconductor, (2) migration of the charge carries toward the surface, and (3) chemical reactions at the surface of the semiconductor making H_2 and O_2 evolution. Those processes demonstrated both the oxidizing sites and the reduction sites on the same catalyst (Fig. 1a). The photons with appropriate energy are harvested by semiconductor to excite electrons from valence band (VB) to conduction band (CB), leaving holes in the VB. Consequently, both electrons and holes are separated and then move towards catalyst's surface, unless they recombine in the bulk or on the surface. At the end, the electrons and holes on surface will allocate to the adsorbed species to initiate corresponding water redox processes, respectively.

Water splitting is thermodynamically not favourable process and an absorption of light having an energy more than (or equal to) the band gap of the photocatalysts that consist of the semiconductor materials in order to drive the reaction forward [6, 8]. Conceptually, the band gap energy should be at least 1.23 eV for overall water oxidation process [9]. Practically, an activation barrier is created when the electron moving between molecules photocatalysts and water. Therefore, the photon energy requires should be greater than the minimum band gap energy in order to perform photocatalytic water splitting [11]. For the hydrogen evolution reaction (HER) and the oxygen evolution reaction (OER) to occur on the catalyst's active sites, the minimum/ bottom of the CB energy level should be located at a more

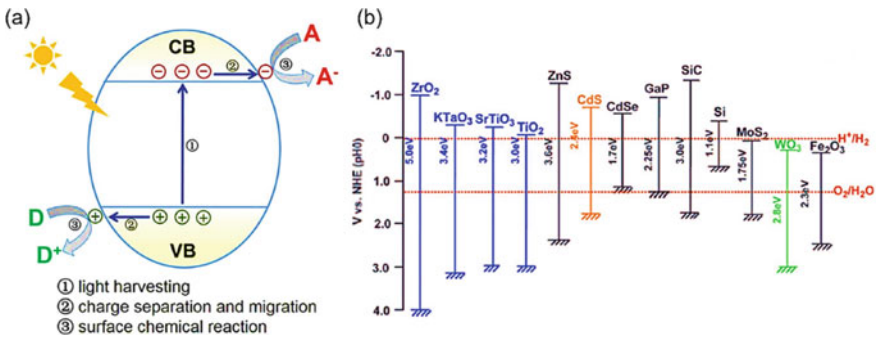

Fig. 1 **a** Schematic illustration for a typical photocatalytic process based on semiconductor [7]; **b** Band structure of semiconductor and redox potential of water splitting [8]

negative than the H_2 evolution potential ($E_{H2}/_{H2O}$, 0 V versus NHE, pH = 0) (Eq. (1)), whereas the maximum/ top of the VB must be more positive than O_2 evolution potential ($E_{2/H2O}$, 1.23 eV vs. NHE, pH = 0) [9] (Eq. (2)).

$$4H^+ + 4e^- \rightarrow 2H_2 \tag{1}$$

$$2H_2O + 4h^+ \rightarrow 4H^+ + O_2 \tag{2}$$

In Fig. 1b, the band positions of various materials are shown. Band engineering is one of the approaches used to design the visible light sensitivity of water splitting materials. Low band gap photocatalytic materials are regularly more sensitive to photon-corrosion as compared to larger band gap materials, but higher band bap are not adept of harvesting visible light [12]. To achieve the target, many researchers are concentrated in band gap modification, including coupled with narrow band gap semiconductors, surface plasmonic effect, dye sensitization in order to improve visible light activity of the semiconductors [13–17]. Meanwhile, heterojunction composite-based photocatalysts can be boosted to obtained apposite band gap alignment for visible light susceptible water splitting [5, 11]. The non-single compound-based photocatalysts are expedient over single material-based photocatalysts as they capable to harvest more visible light than the individual materials. Other than that, heterojunction architecture with appropriate band edge also facilitates an enhanced charge separation [2, 6, 8]. Additionally, the efficient photon absorption, charge carrier transportation, and separation may be attained through physical improvements such as growth of nanostructured photocatalytic materials with various morphologies for high crystallinity and stability, lesser defects, and minimum charge diffusion length [13, 18, 19].

The photocatalytic activity of a substantial is evaluated by solar to hydrogen (STH) energy conversion for overall redox reaction. The STH efficiency is identified as:

$$\text{SHT} = \frac{\text{Output energy}}{\text{Incident solar light energy}} = \frac{r_{H_2} \times \Delta G}{P_{\text{Sun}} \times A_{\text{Geometric}}} \tag{3}$$

where

r_{H_2}	H_2 production rate
ΔG	Gibbs free energy
P_{Sun}	Energy flux of sunlight
$A_{\text{Geometric}}$	Area of reactor

Theoretical r_{H_2} can be counted from the photon's number in the solar spectrum at a different quantum efficiency (QE).

$$\text{QE}(h\upsilon) = \frac{2 \times r_{H_2}}{I_o(h\upsilon)} \tag{4}$$

Hence, hypothetical STH at different QE can be predicted by Eqs. (3) and (4), respectively. For sacrificial agent-assisted water splitting, photo-conversion efficiency (PCE) and incident photon to current conversion efficiency (IPCE) are used which are calculated by Eqs. (5) and (6).

$$\mathrm{PCE} = j_{\mathrm{p}} \times \left(1.23 - \frac{|V|}{I_{\mathrm{o}}}\right) \tag{5}$$

where

j_{p} Photocurrent density at the measured potential
V bias potential versus NHE
I_{o} power density of incident light

$$\mathrm{IPCE} = \frac{1240 \times J}{\lambda \times I_{\mathrm{light}}} \tag{6}$$

where

J Photocurrent density at 0 V at a certain wavelength (λ)
I_{light} Irradiance intensity at λ.

The multiple combines different auspicious properties from various materials, which may also improve physiochemical properties and electronic configuration, hence slow recombination of photo-generated charges, sustain to photo-corrosion, and an appropriate band gap can be achieved, which is possible to reach a targeted STH efficiency. Furthermore, the suitable band alignment and high stability of the photocatalytic material in an aqueous mixture are also tremendously important for the water splitting reaction.

2 Different Type of Junction Used in Photocatalysis

Designation of a suitable semiconductor photocatalyst is the key factor to solve the current energy and environmental issues owing to its ability to maximize solar energy to stimulate various photocatalytic reactions. Hence, it is essential for the beginners/researchers in this field to understand the different type of heterojunctions used in photocatalysis, which include Type-II heterojunction and Z-schemes. Next, we will discuss the difference of each heterojunction.

For Type-II heterojunction, this type of junction is composed of two semiconductors with staggered band structure configuration, as shown in Fig. 2a. Under the incident light with sufficient energy, the electron in photocatalyst I (PC I) (with

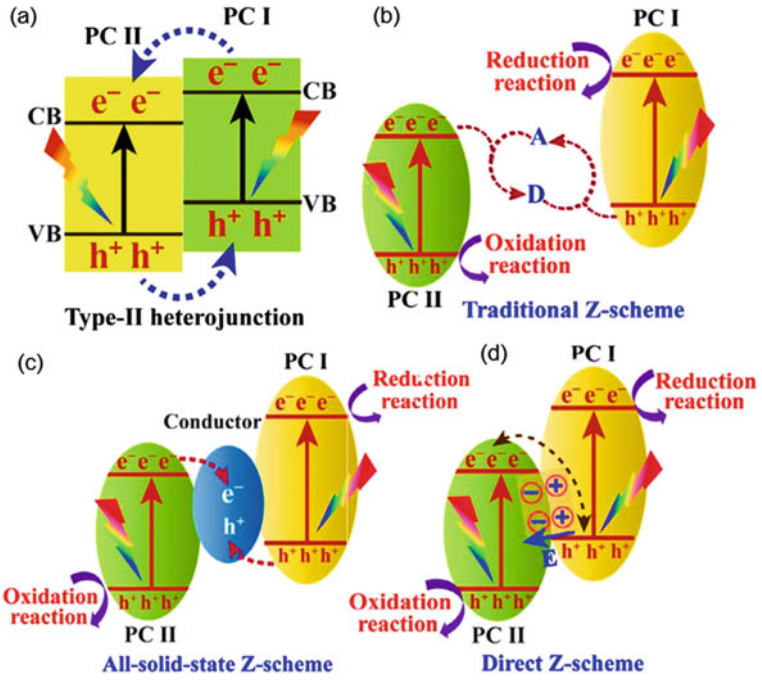

Fig. 2 **a** Schematic illustration of Type-II heterojunction. CB, VB, PC I, and PC II stand for the conduction band, valence band, photocatalyst I and photocatalysts II, respectively, **b** schematic illustration of charge carrier transfer in traditional Z-scheme photocatalysts; A and D stand for electron acceptor and donor, respectively, **c** schematic illustration of charge carrier transfer in all-solid-state Z-scheme photocatalysts, **d** schematic illustration of charge carrier transfer in direct Z-scheme photocatalysts. E means the electric field [20]

higher CB position) will be migrating to photocatalyst II (PC II) (lower CB position). Whilst the holes move in a reverse way, gave rise to an accumulation of holes at PCI for an oxidation reaction and the accumulation of electrons at PC II for a reduction reaction. Although the mentioned effect promotes the spatial separation and suppressed charge recombination, however, this kind of heterojunction may fail to drive a specific photocatalytic reaction [21].

A Z-scheme photocatalyst, in contrast could perform excellent photocatalytic activity owing to (1) simultaneous preservation of strong reduction and oxidation capabilities; (2) spatial separation of oxidative and reductive active sites; (3) high charge separation efficiency; (4) wide spectrum of photocatalysts, and (5) extended light harvesting range. It should be notable that a semiconductor with narrow bandgap should be selected in order to achieve points (4) and (5).

Depending on the type of charge carrier mediator introduced, the Z-scheme photocatalysts are classified into three, one of them is traditional Z-scheme photocatalyst, which is usually composed of two different photocatalysts coupled through a reversible redox ion pair (Fig. 2b), taking examples: Fe^{3+}/Fe^{2+} and IO^{3-}/I^{-} are

used as the charge carriers transfer medium. When the photocatalysts are exposed to light, the electrons generated in CB of PC II are consumed by electron acceptor species while the holes in VB of PC I are consumed by electron donor species. The photogenerated holes in VB of PC II participated in the oxidation reaction, while the electrons in the CB of PCI performed a reductive reaction, hence gave rise to enhance photocatalytic performance. Nevertheless, there are some shortenings of this type of photocatayst, as listed below [22–24]:

i. Redox mediator-induced back reactions are thermodynamically feasible due to the generated electrons and holes with strong redox power are consumable by shuttle redox ion pairs.
ii. Light shielding effect in solution systems.
iii. Slow charge carrier transfer and solution pH sensitivity
iv. Reduced reaction rate due to unstable redox mediators.

While, for all-solid-state Z-scheme photocatalyst, an electron solid conductor (Au, Ag, and Cu NPs) is utilized as a charge transfer bridging in all-solid-state Z-scheme photocatalyst (Fig. 2c). Typically, noble metals are commonly employed as excellent electron mediators, in addition, graphene, CNTs, etc. are also good for photocatalytic performance and stability performance. The all-solid-state Z-scheme photocatalysts are viable to work in both liquid and gas phases, ascribed to the solid conductor prompted for a fast charge carrier transfer. However, the problems of this photocatalyst would be the expensive noble metals and its shielding effect [23, 25–28].

Lastly, a direct-Z-scheme photocatalyst is meant for a direct contact between two semiconductors without the need of charge carrier transfer mediator [29–33]. As shown in Fig. 2d, both the semiconductors are in close contact without any mediator, which resulted in suppressed backward reactions, shielding effects, and resistant to corrosion. In this case, a work function difference between both photocatalysts is important to induce charge redistribution and to form internal electric field, which is significantly affect the charge carrier separation and transfer process [34, 35].

To fully understand the mechanisms, there are two types of photocatalytic systems to be discussed, which are (i) PC I has a higher CB and VB positions and smaller work function (higher Fermi level) than PC II, and (ii) typical p–n junction. For the first case (Fig. 3a), free electrons of PC I can be easily transfer to PC II when PC I and PC II are in contact until their Fermi levels are equilibrated (Fig. 3b). Hence, a built-in electric field and a band edge bending are formed, attributed to the PC I side is positively charged, while negatively charged at the PC II interface. The Z-scheme charge transfer mode is much in favour for this case. The existence of internal electric field favors the recombination between the photogenerated electrons in the CB of PC II and photogenerated holes in the VB of PC I [36] (Fig. 3c). The factors such as internal electric field, the extra potential barrier induced from band bending, and Coulomb repulsion hinder the transferred of photogenerated electrons from the CB of PC I to PC II CB, as well as the transfer of photogenerated holes (Fig. 3d).

Meanwhile, the electrons from the CB of PC I and holes from the VB of PC II are maintained and spatially separated, in addition, they can participate in specific

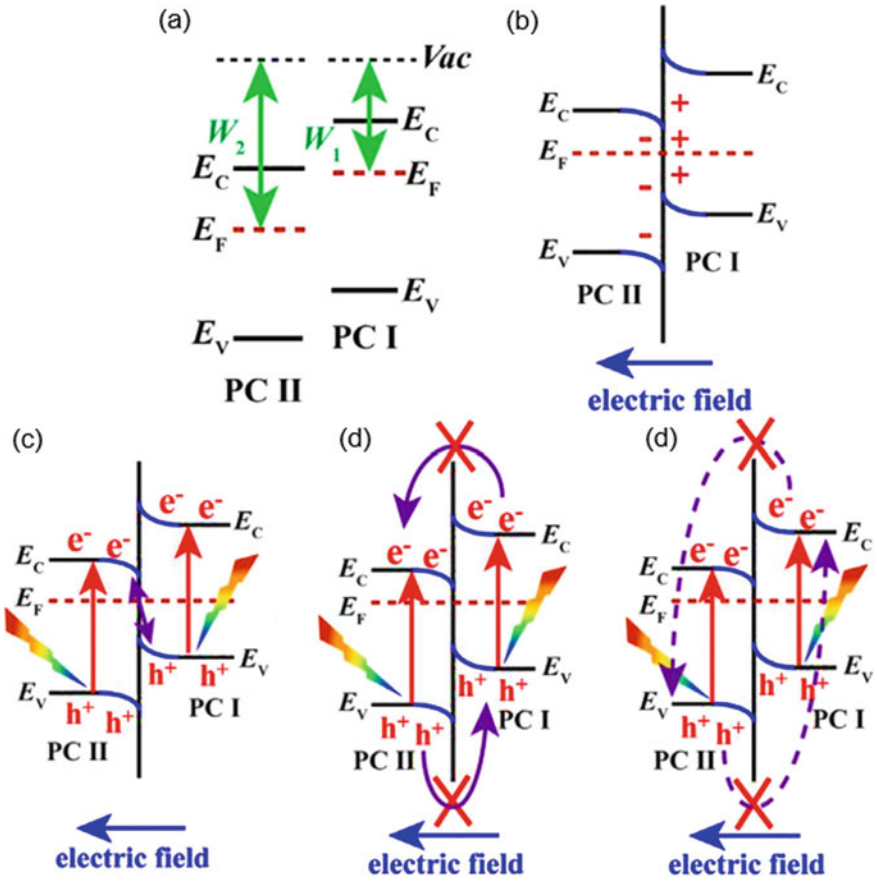

Fig. 3 Schematic illustration of semiconductor–semiconductor junction with staggered band configurations ($W_1 < W_2$) [18]: **a** before contact, **b** in contact, **c** photogenerated charge carrier transfer process in direct Z-scheme mode, **d** photogenerated charge carrier transfer process in Type-II mode, and **e** photogenerated charge carrier recombination. W_1 and W_2 denote the work function of PC I and PC II, respectively. V_{ac}, E_c, E_v, and E_F stand for the vacuum level, conduction band minimum, valence band maximum, and Fermi level, respectively

reductive and oxidative photocatalytic reactions, respectively. It is worth noting that the induced electric field can suppress the recombination between the photogenerated electrons in the CB of PC I and the photogenerated holes in the VB of PC II, as shown in Fig. 3e. In contrast, the second type of the system, p–n junction (Fig. 4a), is significantly different from the first one (Fig. 3a). When p-type semiconductor is contacted with the n-type semiconductor, free electrons of n-type semiconductor can be transferred to p-type semiconductor to form a built-in electric field (Fig. 4b). Under this circumstance, a p–n junction charge carrier transfer mode (Fig. 5c) is formed rather than direct Z-scheme charge carrier transfer mode (Fig. 4d) owing to the existed built-in electric field [37, 38]. Thus, the photogenerated charge carrier

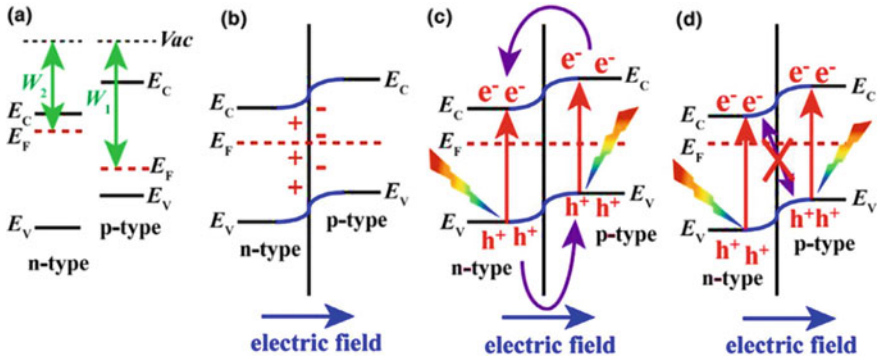

Fig. 4 Schematic illustration of p–n junction [18]: **a** before contact, **b** in contact, **c** transfer of photogenerated charge carriers in p–n junction mode, and **d** not-allowed transfer of photogenerated charge carriers in direct Z-scheme mode

transfer mode in p–n junction is unflavored for direct Z-scheme mode (Fig. 4c and d).

Similar to direct Z-scheme photocatalysts, all-solid-state photocatalysts exhibiting similar VB and CB edge bending. At the metal–semiconductor interface of all-solid-state photocatalysts, the free electrons will be migrated from a semiconductor to a metal when metal has larger work function than the semiconductor, resulted in an upward bent semiconductor band induced by an electric field [23, 25]. Nevertheless, when metal has smaller work function than semiconductor, the free electrons will then be migrated from a metal to a semiconductor, which led to a downward bending of semiconductor band edge. While for the traditional Z-scheme photocatalysts, free electron redistribution would not be occurring (no internal electric field between them) because there isn't direct contact between two different photocatalysts in the presence of an appropriate shuttle redox ion mediator [31]. Hence, the VB and CB edges of each component are not affected when traditional Z-scheme photocatalysts are formed.

3 Why Semiconductor in Photocatalytic Hydrogen Production

Why semiconductor for photocatalysis? Semiconductor-based photocatalysis such as TiO_2 (the most commonly reported) has emerged as an effective photocatalyst for various applications owing to its renewable, clean, and safe technology where photocatalyst requires only solar energy as the prime energy source [39, 40]. The pioneering work of TiO_2 semiconductor photocatalysis was initiated by Fujishima and Honda for photochemical water splitting [9]. TiO_2 based two dimensional (2D) nanosheets are derived from the exfoliation of titanate layer. Although it exhibits

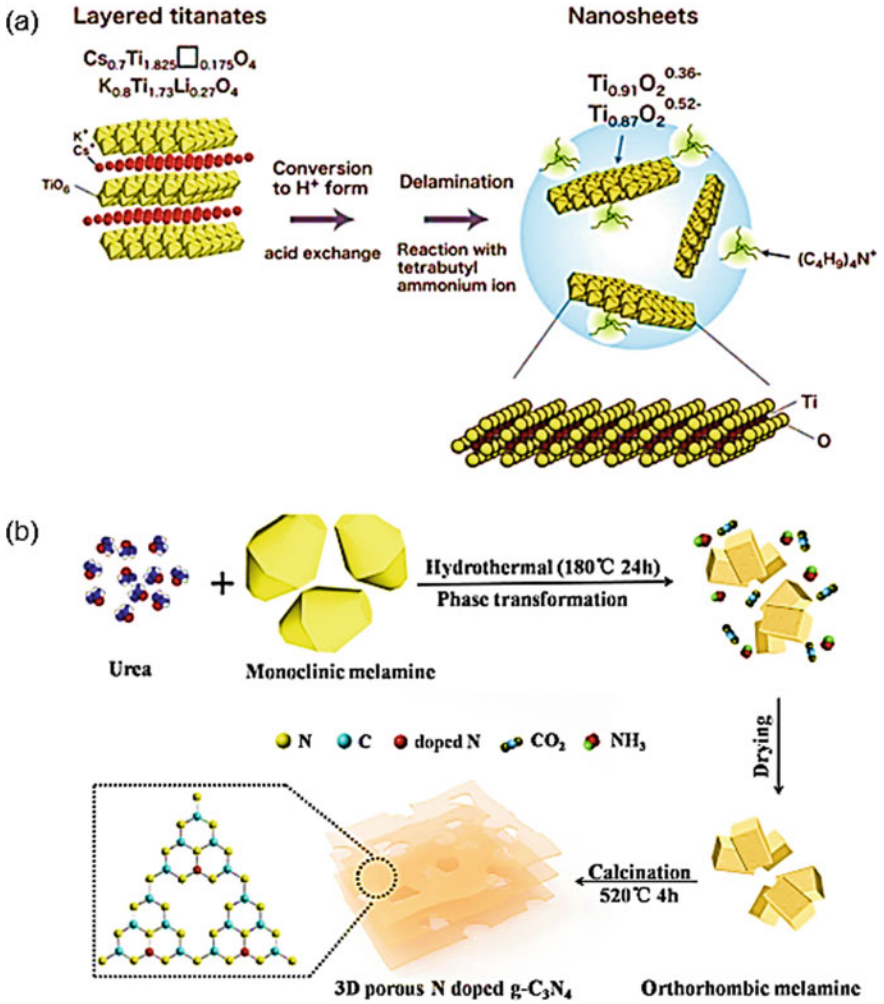

Fig. 5 **a** Schematic illustration of the crystal structure of a typical lepidocrocite-type titanate and its exfoliation into 2D titania nanosheets [43], **b** Schematic illustration for the formation of 3D ultrathin porous N-doped g-C_3N_4 [44]

similar properties as rutile and anatase TiO_2, however, it has larger band gap due to the size quantization. Taking an example, $Ti_{0.91}O_2^{0.36-}$ nanosheets has a band gap of 3.8 eV, as compared to anatase TiO_2 with a band gap of 3.2 eV [41]. Usually layered titanates are prepared through high temperature solid state reaction of a mixture of TiO_2 and alkali metal carbonates, subsequently processed with acidic solution to form protonated intermediate via ion-exchange process (Fig. 5a). In addition, other layered metal oxides nanosheets such as WO_3, titanoniobate, and perovskite oxides are also

prepared through high temperature solid state reactions and wet-chemical exfoliation processes, where high temperature synthesis process is unfavouring industrial purpose.

Doping of TiO_2 has been showing effective approach to extend light absorption to visible region, however, low photocatalytic efficiency due to rapid charge recombination could be the main challenge of the existing photocatalysts [42]. Thus, to overcome the recombination issue and to improve charge separation, developing a suitable semiconductor composites or engineering a 2D material such as graphene or graphitic carbon nitride (g-C_3N_4) is one of the best options. The g-C_3N_4 is denoted as the most stable allotrope among the carbon nitride and g-C_3N_4 exists in the form of 2D sheets consisting of tri-s-triazines interconnected with tertiary amines. What is the difference between TiO_2 and g–C_3N_4? Unlike TiO_2 (active in UV region), g-C_3N_4 is a visible light active photocatalyst due to its bandgap of ca. 2.7 eV with a suitable conduction and valence band positions. In addition, g-C_3N_4 is thermally and chemically stable in most solvents such as water, alcohols, DMF, THF, diethyl ether, and toluene.

Recently, ultrathin 2D g-C_3N_4 has attracted consideration attentions due to its large specific surface area, and low carrier recombination properties, which thus demonstrated superior potential for electronics, energy conversion and storage applications. A highly anisotropic 2D g-C_3N_4 nanosheets prepared through a top-down strategy (thermal oxidation etching of bulk g-C_3N_4 in air) has demonstrated a high specific surface area of 306 m^2g^{-1}, accompanied with larger band gap, thus improved electron transport ability along the in-plane direction, increased photoexcited charge carrier lifetime, and excellent photocatalytic activities than bulk g-C_3N_4 [45]. Nevertheless, the 2D g-C_3N_4 nanosheets usually suffer from severe restacking problem, which is highly detrimental to the photocatalytic activity. Thus, owing to its tunable morphologies, g-C_3N_4 is highly favored in producing an enlarged specific surface area, improved charge transfer efficiency and surface catalytic reaction. In accord to the advantages of three dimensional (3D) porous structure, superior photocatalytic performance has been reported for a 3D mesoporous g-C_3N_4. This photocatalyst, in short denoted as UM3 has shown remarkable photocatalytic H_2 evolution performance and stability, as compared to the pristine (Fig. 5b). Hence, the research on developing more potential semiconductors which is cost-effective, efficient in photocatalytic activity and charge transport is still ongoing.

4 Facile Developments of Photocatalyst for Water Splitting

Despite the TiO_2 has demonstrated improved photocatalytic activity towards water-splitting, its efficiency is still far underneath the prerequisite for commercialization due to the inherent constraint of TiO_2. Hence, the researchers have been concentrated to create other potential cocatalysts to improve the productivity of water-splitting reaction. The photocatalysts combined with at least two elements for H_2 evolution through photocatalytic water splitting that are more active than

TiO_2. For instant, Liu et al. [46] reported efficient Au–Cu/TiO_2/MoS_2 composite photocatalyst for H_2 production through water splitting. Firstly, TiO_2 nanosheets were blended, at that point hybridized them with MoS_2 nanosheets by a simple aqueous solution. Subsequently, the Au-Cu nanoparticles were effectively inserted into the TiO_2/MoS_2 composite by a refluxing technique followed by calcination, lastly obtained TiO_2/MoS_2/Au-Cu ternary composite catalyst. The balanced mixture of the ternary composite improves the photocatalytic efficiency and leds the separation of photo-induced electron–hole separation. Zhao et al. [47] synthesized NiO-TiO_{2-x}/C photocatalysts for H_2 production through water splitting. Because of the cooperative energy of carbon nanosheets, NiO, and TiO_2, the optimum (1 wt.%) NiO-TiO_{2-x}/C-T650 nanocomposites was demonstrated efficient photocatalytic hydrogen evolution from water, beating 18-fold in efficiency higher than TiO_2/C. However, NiO/TiO_2 nanoparticles generates agglomerate into enormous bunches, obstructing effective photo-induced electron transfer, which reduces a space of NiO/TiO_2 p-n heterojunctions for the photocatalytic reaction.

Stabilization of Cu_2O onto TiO_2 was reported by Wei et al. [48] by adjustment of crystal facets and defects of TiO_2 (Fig. 6). Both experimental and hypothetical conception demonstrated that 101-faceted TiO_2 could make electron importing channel into the Z-scheme system. The Cu_2O/TiO_2 heterostructures with {101} facet was reported to be 251-fold activity for photo-induced water splitting reaction compared with other facets, along with high stability. However, the impact of defect in Z-scheme system on the stability of Cu_2O should be investigate in detail for H_2 evolution.

Some different semiconductors, for example, Nb_2O_5, NiO–GO, NiO–TiO_2, Pt/RuO_2 and $SrTiO_3$ were demonstrated to show photocatalytic water splitting [49–51]. However, the proficiency of these mass photocatalysts is restricted by active sites of reaction and low change transfer efficiency because of the electron/hole recombination. In this manner, discovering steady and productive photocatalyst materials actually stays challenging. Two dimensional materials which have been an interesting issue in a decade ago, presenting tunable electronic and optical properties that make them promising candidates for water splitting [52]. A few exploratory examinations have demonstrated that 2D material-based photocatalysts display exceptionally

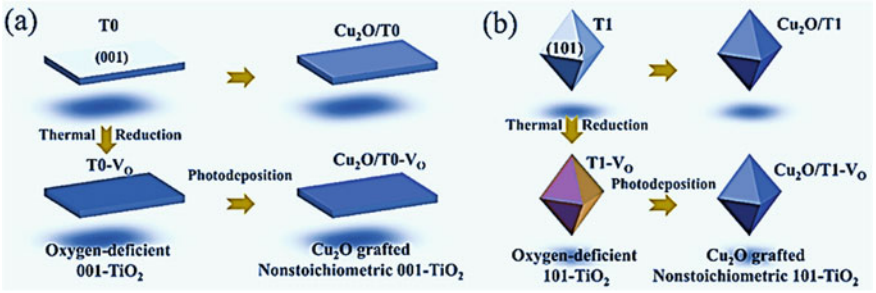

Fig. 6 Schematic illustration of synthetic routes for Cu_2O/TiO_2 heterostructures [48]

improved photocatalytic activities contrasted with the conventional bulk materials [53, 54].

To overcome the photocorrosion issue of composite photocatalyst while keeping up its high effectiveness, a photocatalytic framework called Z-scheme, which imitates the Z-scheme system in the characteristic photosynthesis of green plants, has been created to produce H_2 and O_2 at the same time. The Z-scheme is a double photocatalyst framework that fundamentally comprises of a H_2-photocatalyst and an O_2-photocatalyst to perform water reduction and oxidation, individually. Wen et al. [55] synthesized ZnO coupled with g-C_3N_4 to create direct Z-scheme, photocatalytic systems attributable to their well-matched band positions. The outcomes affirmed that the inserted Au NPs act as an electron mediator to advance vectorial electron move in direct Z-scheme ZnO/g-C_3N_4 heterojunction. Recently, some works reported that the ZnO/TiO_2 heterojunctions demonstrated increased photocatalytic activity due to their matched energy band alignments and high electron mobility of ZnO that efficiently promote the carrier separation and transfer [56]. However, the reported ZnO/TiO_2 heterostructures were usually sealed structures with lower surface areas, such as the core–shell structured ZnO/TiO_2 or branched ZnO/TiO_2 and disordered ZnO rods due to the aggregation of ZnO seeds on the TiO_2 nanorods, which result in the obstruction of light absorption for TiO_2, usually demonstrating unsatisfactory water splitting performance. Besides, ZnO also suffers from the low photocorrosion resistance in most electrolytic media and the morphologies and structures of ZnO seriously affect the photostabilities of the ZnO/TiO_2 heterojunctions.

Niu et al. [57] evaluated the photogenerated electrons/holes recombination properties of C_3N/C_3B catalyst and compared the performance for H_2 generation through water splitting. The 2D C_3N/C_3B p-n heterostructure was found to be promising metal free Z-scheme photocatalyst for water splitting reaction. The strong redox ability of C_3B and C_3N layers are driving force to split water without addition of overpotential or co-catalyst. Bismuth-based oxides have attracted attention in photocatalytic water splitting because of their high dielectric permittivity, reasonable band structure (2.8 eV) and position of valence band [58]. The Z-scheme photocatalyst offer successful charge seperation and move without adding any sacrificial reagent. Nitrogen/fluorine codoping decreases the defect concentration, which reduced the recombination of photoexcited electrons, contrasted with nitrogen-doped photocatalyst. It has been suggested that fluorine doping into TiO_2 improved its photocatalytic water splitting under UV illumination by supressing recombination of electron/hole. Miyoshi et al. [59] compared the activity of nano-TiO_2:N,F and TiO_2:N,F in Z-scheme system under visible light irradiated Z-scheme water-splitting. It was concluded that Z-scheme system of TiO_2:N,F was found to increase fourfold compared to the bulk TiO_2:N,F. While TiO_2:N,F in Z-scheme system has been reported more effective than bulk TiO_2:N,F, the impact of TiO_2:N,F molecule size remain unknown.

Utilization of Nanostructured Si essentially improves the solar H_2 conversion proficiency of an ideal photoelectrochemical system. Oh et al. [60] demonstrated that the water splitting efficiency of nanoporous ‘black’ Si was more than the polished Si electrode. In similar, n-type nano-Si appeared about 20% improvement in quantum

efficiency because of the decreased reflectance and high photocorrosion in concentrated HI. Recently, n-type Si nanowire demonstrated the high water splitting activity, contrasted with the planar Si, in the presence of Br_2/Br solution. Zhang et al. [61] investigated the activity of water splitting by running Si photocatalyst. It has been reported that the photocatalytic hydrogen development execution of silicon catalyst incredibly impacts on a surface functional group of catalyst. This outcome is consistent with the information proclaimed by Rye et al. [62] who endeavored to synthesized Pt/Si photocatalyst for H_2 production through water splitting. Nonetheless, the costly platinum co-catalyst remains challenge for real application.

There is a basic postulation that the H atoms on Si surface are electron-deficient and may fill in as an electron sink to improve charge separation. Similar phenomenon has been discussed by other researchers and reported that oxidation occurs on Si–OH and H_2 produces on Si–H surfaces by reduction process, as shown the Eqs. (7–9):

$$\text{Oxidation} : h^+ + \text{Si} + H_2O \rightarrow \text{Si} - \text{OH} + H^+ \tag{7}$$

$$\text{Reduction} : e^- + \text{Si} - \text{H} + H^+ \rightarrow \text{Si} + H_2 \tag{8}$$

$$\text{Reduction} : e^- + \text{Si} - \text{OH} + H^+ \rightarrow \text{Si} + H_2O \tag{9}$$

The function of photogenerated electron and holes on the photocatalyst is schematically shown in Fig. 7. The function of photogenerated electrons on Si photocatalyst could be elucidated based on the dynamic charge separation [63, 64]. As recently revealed the ultrathin layer of catalyst led the detachment of photogenerated electrons

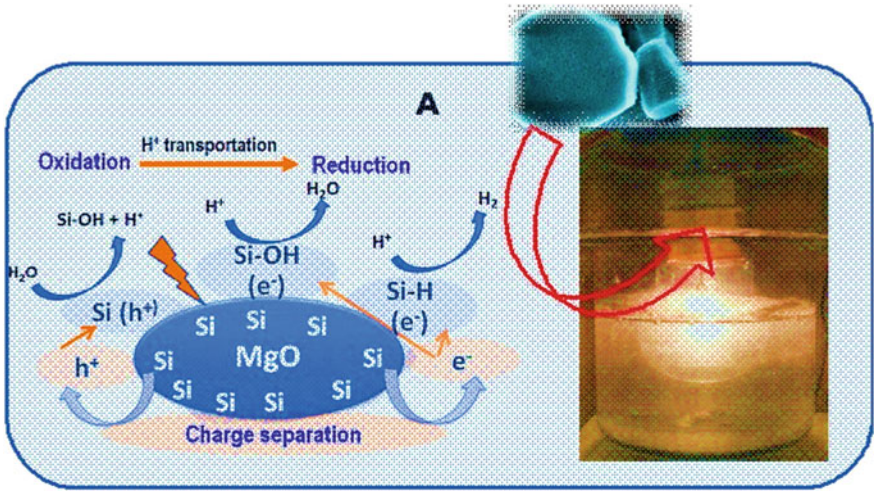

Fig. 7 Water splitting mechanism on Si photocatalyst [63]

because of intrinsic effect of Si [65]. While conceding to this conceivable explanation, there is still need to investigate the molecular interaction and kinetic of carriers for photocatalytic water splitting reaction.

5 Conclusion

In the course of recent years, a few semiconductor materials and photocatalytic frameworks have been produced for the water-splitting irradiation under UV and visible light. It has been seen that photo-induced charge separation, avoidance of water-splitting in reverse reaction, and use of a wide range of light energy are the basic prerequisites for accomplishing high proficiency of water splitting. The high evolution of H_2 energy through water splitting has been evident by the addition of sacrificial reagent that could supress the openings to repress charge recombination. In any case, to accomplish feasible hydrogen evolution, sacrificial reagent must be persistently added during reaction. Besides, photocatalytic reactor design to accomplish separate H_2 and O_2 development, for example, the H-type reactor and the novel Z-scheme, should be required for efficient hydrogen production. Different strategies, for example, potentially doping of metal or metal oxide particles on the photocatalyst have been effectively utilized to improve the performance of photocatalytic reaction. Photocatalytic water splitting is a cross-discipline innovation that requires the contribution of specialists from various fields (i.e., scientific experts, electrical architects, material researchers, and physicists). The advancement of new innovations requires cooperation with a solid hypothetical foundation for a superior comprehension of the hydrogen production catalyst so as to think of a minimal effort for hydrogen evolution.

Acknowledgements The authors acknowledge the financial support of the Impact Research Scheme (SPB, Project Number: SP0005-2020) from UMS Research Grant, Universiti Malaysia Sabah.

References

1. Razek SA, Popeil MR, Wangoh L et al (2020) Designing catalysts for water splitting based on electronic structure considerations. Electron Struct 2:023001. https://doi.org/10.1088/2516-1075/ab7d86
2. Lin L, Hisatomi T, Chen S et al (2020) Visible-light-driven photocatalytic water splitting: recent progress and challenges. Trends Chem 2:813–824. https://doi.org/10.1016/j.trechm.2020.06.006
3. Safari F, Dincer I (2020) A review and comparative evaluation of thermochemical water splitting cycles for hydrogen production. Energy Convers Manag 205:112182. https://doi.org/10.1016/j.enconman.2019.112182

4. Chen Y, Ji S, Sun W et al (2020) Engineering the atomic interface with single platinum atoms for enhanced photocatalytic hydrogen production. Angew Chemie—Int Ed 59:1295–1301. https://doi.org/10.1002/anie.201912439
5. Miseki Y, Sayama K (2019) Photocatalytic water splitting for solar hydrogen production using the carbonate effect and the Z-Scheme reaction. Adv Energy Mater 9:1–15. https://doi.org/10.1002/aenm.201801294
6. Kumaravel V, Mathew S, Bartlett J, Pillai SC (2019) Photocatalytic hydrogen production using metal doped TiO_2: a review of recent advances. Appl Catal B Environ 244:1021–1064. https://doi.org/10.1016/j.apcatb.2018.11.080
7. Zhang N, Gao C, Xiong Y (2019) Defect engineering: a versatile tool for tuning the activation of key molecules in photocatalytic reactions. J Energy Chem 37:43–57. https://doi.org/10.1016/j.jechem.2018.09.010
8. Kudo A, Miseki Y (2009) Heterogeneous photocatalyst materials for water splitting. Chem Soc Rev 38:253–278. https://doi.org/10.1039/b800489g
9. Fujishima A, Honda K (1972) Electrochemical photolysis of water at a semiconductor electrode. Nature 238:37–38. https://doi.org/10.1038/238037a0
10. Wang Y, Vogel A, Sachs M et al (2019) Current understanding and challenges of solar-driven hydrogen generation using polymeric photocatalysts. Nat Energy 4:746–760. https://doi.org/10.1038/s41560-019-0456-5
11. Maeda K (2011) Photocatalytic water splitting using semiconductor particles: history and recent developments. J Photochem Photobiol C Photochem Rev 12:237–268. https://doi.org/10.1016/j.jphotochemrev.2011.07.001
12. Su J, Guo L, Bao N, Grimes CA (2011) Nanostructured WO3/BiVO4 heterojunction films for efficient photoelectrochemical water splitting. Nano Lett 11:1928–1933. https://doi.org/10.1021/nl2000743
13. Kudo A (2013) New materials for photocatalytic and photoelectrochemical water splitting. AIP Conf Proc 1568:7–10. https://doi.org/10.1063/1.4848079
14. Domen K, Kondo JN, Hara M, Takata T (2000) Photo-and mechano-catalytic overall water splitting reactions to form hydrogen and oxygen on heterogeneous catalysts. Bull Chem Soc Jpn 73:1307–1331
15. Domen K, Hara M, Kondo JN et al (2001) New aspects of heterogeneous photocatalysts for water decomposition. Korean J Chem Eng 18:862–866. https://doi.org/10.1007/BF02705609
16. Kudo A (2006) Development of photocatalyst materials for water splitting. Int J Hydrogen Energy 197–202
17. Maeda K, Domen K (2007) New non-oxide photocatalysts designed for overall water splitting under visible light. J Phys Chem C 111:7851–7861. https://doi.org/10.1021/jp070911w
18. Xu Q, Zhang L, Yu J et al (2018) Direct Z-scheme photocatalysts: principles, synthesis, and applications. Mater Today 21:1042–1063. https://doi.org/10.1016/j.mattod.2018.04.008
19. Yuan Y, Lv J, Jiang X et al (2007) Large impact of strontium substitution on photocatalytic water splitting activity of $BaSnO_3$. Appl Phys Lett 91:27–30. https://doi.org/10.1063/1.2778631
20. Low J, Yu J, Jaroniec M et al (2017) Heterojunction photocatalysts. Adv Mater 29:1–20. https://doi.org/10.1002/adma.201601694
21. Bai S, Jiang J, Zhang Q, Xiong Y (2015) Steering charge kinetics in photocatalysis: Intersection of materials syntheses, characterization techniques and theoretical simulations. Chem Soc Rev 44:2893–2939. https://doi.org/10.1039/c5cs00064e
22. Maeda K (2013) Z-scheme water splitting using two different semiconductor photocatalysts. ACS Catal 3:1486–1503. https://doi.org/10.1021/cs4002089
23. Zhou P, Yu J, Jaroniec M (2014) All-solid-state Z-scheme photocatalytic systems. Adv Mater 26:4920–4935. https://doi.org/10.1002/adma.201400288
24. Bala Chandran R, Breen S, Shao Y et al (2018) Evaluating particle-suspension reactor designs for Z-scheme solar water splitting via transport and kinetic modeling. Energy Environ Sci 11:115–135. https://doi.org/10.1039/c7ee01360d

25. Li H, Tu W, Zhou Y, Zou Z (2016) Z-Scheme Photocatalytic systems for promoting photocatalytic performance: recent progress and future challenges. Adv Sci 3. https://doi.org/10.1002/advs.201500389
26. Iwase A, Ng YH, Ishiguro Y, et al (2011) Reduced graphene oxide as a solid-state electron mediator in Z- scheme photocatalytic water splitting under visible light. Am Chem Soc. pp 11054–11057
27. Li H, Yu H, Quan X et al (2016) Uncovering the key role of the fermi level of the electron mediator in a Z-Scheme photocatalyst by detecting the charge transfer process of WO3-metal-gC3N4 (Metal = Cu, Ag, Au). ACS Appl Mater Interfaces 8:2111–2119
28. Li X, Yan X, Lu X et al (2018) Photo-assisted selective catalytic reduction of NO by Z-scheme natural clay based photocatalyst: insight into the effect of graphene coupling. J Catal 357:59–68. https://doi.org/10.1016/j.jcat.2017.10.024
29. Jia Q, Iwase A, Kudo A (2014) BiVO4-Ru/SrTiO3: Rh composite Z-scheme photocatalyst for solar water splitting. Chem Sci 5:1513–1519. https://doi.org/10.1039/c3sc52810c
30. Song H, Yu YT, Norby P (2009) Efficient complete oxidation of acetaldehyde into CO2 over Au/TiO 2 core-shell nano catalyst under UV and visible light irradiation. J Nanosci Nanotechnol 9:5891–5897. https://doi.org/10.1166/jnn.2009.1263
31. Liu X, Chen N, Li Y et al (2016) A general nonaqueous sol-gel route to g-$C3N_4$-coupling photocatalysts: the case of Z-scheme g-$C3N_4$/TiO_2 with enhanced photodegradation toward RhB under visible-light. Sci Rep 6:1–16. https://doi.org/10.1038/srep39531
32. Zhou D, Chen Z, Yang Q et al (2016) Facile construction of g-$C3N_4$ nanosheets/TiO_2 Nanotube Arrays as Z-scheme photocatalyst with enhanced visible-light performance. ChemCatChem 8:3064–3073. https://doi.org/10.1002/cctc.201600828
33. Luo J, Zhou X, Ma L et al (2016) Enhancing visible light photocatalytic activity of direct Z-scheme SnS_2/Ag_3PO_4 heterojunction photocatalysts. Mater Res Bull 81:16–26. https://doi.org/10.1016/j.materresbull.2016.04.028
34. Cui J, Li Y, Liu L et al (2015) Near-infrared plasmonic-enhanced solar energy harvest for highly efficient photocatalytic reactions. Nano Lett 15:6295–6301. https://doi.org/10.1021/acs.nanolett.5b00950
35. Liu J, Cheng B, Yu J (2016) A new understanding of the photocatalytic mechanism of the direct Z-scheme g-C_3N_4/TiO_2 heterostructure. Phys Chem Chem Phys 18:31175–31183. https://doi.org/10.1039/c6cp06147h
36. Zhang L, Li S, Liu B, et al (2014) Highly efficient CdS / WO 3 photocatalysts : Z- scheme photocatalytic mechanism for their enhanced photocatalytic H 2 evolution under visible light
37. Zheng L, Zheng Y, Chen C et al (2009) Network structured SnO_2/ZnO heterojunction nanocatalyst with high photocatalytic activity. Inorg Chem 48:1819–1825. https://doi.org/10.1021/ic802293p
38. Son DY, Im JH, Kim HS, Park NG (2014) 11% efficient perovskite solar cell based on ZnO nanorods: an effective charge collection system. J Phys Chem C 118:16567–16573. https://doi.org/10.1021/jp412407j
39. Bard AJ (1980) Photoelectrochemistry. 207:139–144
40. Hoffmann MR, Martin ST, Choi W, Bahnemann DW (1995) Environmental applications of semiconductor photocatalysis. Chem Rev 95:69–96. https://doi.org/10.1021/cr00033a004
41. Sakai N, Ebina Y, Takada K, Sasaki T (2004) Electronic band structure of titania semiconductor nanosheets revealed by electrochemical and photoelectrochemical studies. J Am Chem Soc 126:5851–5858
42. Cao S, Low J, Yu J, Jaroniec M (2015) Polymeric photocatalysts based on graphitic carbon nitride. Adv Mater 27:2150–2176. https://doi.org/10.1002/adma.201500033
43. Luo B, Liu G, Wang L (2016) Recent advances in 2D materials for photocatalysis. Nanoscale 8:6904–6920. https://doi.org/10.1039/c6nr00546b
44. Tian N, Zhang Y, Li X et al (2017) Precursor-reforming protocol to 3D mesoporous g-C3N4 established by ultrathin self-doped nanosheets for superior hydrogen evolution. Nano Energy 38:72–81. https://doi.org/10.1016/j.nanoen.2017.05.038

45. Niu P, Zhang L, Liu G, Cheng HM (2012) Graphene-like carbon nitride nanosheets for improved photocatalytic activities. Adv Funct Mater 22:4763–4770. https://doi.org/10.1002/adfm.201200922
46. Liu Y, Xu C, Xie Y, et al (2020) Au–Cu nanoalloy/TiO2/MoS2 ternary hybrid with enhanced photocatalytic hydrogen production. J Alloys Compd 820.https://doi.org/10.1016/j.jallcom.2019.153440
47. Zhao X, Xie W, Deng Z et al (2020) Salt templated synthesis of NiO/TiO_2 supported carbon nanosheets for photocatalytic hydrogen production. Colloids Surfaces A Physicochem Eng Asp 587:124365. https://doi.org/10.1016/j.colsurfa.2019.124365
48. Wei T, Zhu YN, An X et al (2019) Defect modulation of Z-Scheme TiO_2/Cu_2O photocatalysts for durable water splitting. ACS Catal 9:8346–8354. https://doi.org/10.1021/acscatal.9b01786
49. Ghouri MI, Ahmed E, Ali A et al (2020) The synergistic role of ternary combined semiconductors (Nb_2O_5–MoS_2-MO) hetrojunctions in photocatalytic water splitting. Mater Chem Phys 255:123320. https://doi.org/10.1016/j.matchemphys.2020.123320
50. Nogueira AE, Silva GTST, Oliveira JA et al (2020) CuO decoration controls Nb_2O_5 photocatalyst selectivity in CO_2 reduction. ACS Appl Energy Mater 3:7629–7636. https://doi.org/10.1021/acsaem.0c01047
51. Fo Y, Wang M, Ma Y et al (2020) Origin of highly efficient photocatalyst NiO/$SrTiO_3$ for overall water splitting: insights from density functional theory calculations. J Solid State Chem 292:121683. https://doi.org/10.1016/j.jssc.2020.121683
52. Faraji M, Yousefi M, Yousefzadeh S et al (2019) Two-dimensional materials in semiconductor photoelectrocatalytic systems for water splitting. Energy Environ Sci 12:59–95. https://doi.org/10.1039/c8ee00886h
53. Fu CF, Sun J, Luo Q et al (2018) Intrinsic electric fields in two-dimensional materials boost the solar-to-hydrogen efficiency for photocatalytic water splitting. Nano Lett 18:6312–6317. https://doi.org/10.1021/acs.nanolett.8b02561
54. Lv X, Wei W, Sun Q et al (2017) Two-dimensional germanium monochalcogenides for photocatalytic water splitting with high carrier mobility. Appl Catal B Environ 217:275–284. https://doi.org/10.1016/j.apcatb.2017.05.087
55. Wen P, Sun Y, Li H et al (2020) A highly active three-dimensional Z-scheme ZnO/Au/g-$C3N_4$ photocathode for efficient photoelectrochemical water splitting. Appl Catal B Environ 263:118180. https://doi.org/10.1016/j.apcatb.2019.118180
56. Zhou T, Wang J, Chen S et al (2020) Bird-nest structured ZnO/TiO_2 as a direct Z-scheme photoanode with enhanced light harvesting and carriers kinetics for highly efficient and stable photoelectrochemical water splitting. Appl Catal B Environ 267:118599. https://doi.org/10.1016/j.apcatb.2020.118599
57. Niu X, Bai X, Zhou Z, Wang J (2020) Rational design and characterization of direct Z-Scheme photocatalyst for overall water splitting from excited state dynamics simulations. ACS Catal 10:1976–1983. https://doi.org/10.1021/acscatal.9b04753
58. Ma Y, Jiang X, Sun R, et al (2020) Z-scheme Bi2O2.33/Bi2S3 heterojunction nanostructures for photocatalytic overall water splitting. Chem Eng J 382:123020. https://doi.org/10.1016/j.cej.2019.123020
59. Miyoshi A, Miyoshi A, Kato K et al (2020) Nano: Versus bulk rutile TiO2:N, F in Z-scheme overall water splitting under visible light. J Mater Chem A 8:11996–12002. https://doi.org/10.1039/d0ta04450d
60. Oh J, Deutsch TG, Yuan HC, Branz HM (2011) Nanoporous black silicon photocathode for H2 production by photoelectrochemical water splitting. Energy Environ Sci 4:1690–1694. https://doi.org/10.1039/c1ee01124c
61. Zhang RQ, Liu XM, Wen Z, Jiang Q (2011) Prediction of silicon nanowires as photocatalysts for water splitting: band structures calculated using density functional theory. J Phys Chem C 115:3425–3428. https://doi.org/10.1021/jp111182c
62. Ryu J, Jang YJ, Choi S et al (2016) All-in-one synthesis of mesoporous silicon nanosheets from natural clay and their applicability to hydrogen evolution. NPG Asia Mater 8:e248–e249. https://doi.org/10.1038/am.2016.35

63. Islam A, Teo SH, Awual MR, Taufiq-Yap YH (2020) Assessment of clean H_2 energy production from water using novel silicon photocatalyst. J Clean Prod 244:1–12. https://doi.org/10.1016/j.jclepro.2019.118805
64. Islam A, Teo SH, Awual MR, Taufiq-Yap YH (2019) Improving the hydrogen production from water over MgO promoted Ni–Si/CNTs photocatalyst. J Clean Prod 238. https://doi.org/10.1016/j.jclepro.2019.117887
65. Islam A, Teo SH, Awual MR, Taufiq-Yap YH (2020) Ultrathin assembles of porous array for enhanced H2 evolution. Sci Rep 10:1–14. https://doi.org/10.1038/s41598-020-59325-4